Journal of Sound and Vibration (1998) **209**(5), 753–769

DOUBLE DEGENERACY AND CHAOS IN A RATE GYRO WITH FEEDBACK CONTROL

Z.-M. GE AND H.-H. CHEN

Department of Mechanical Engineering, National Chiao Tung University, Hsinchu, Taiwan, Republic of China

(*Received* 8 *August* 1996, *and in final form* 8 *August* 1997)

The analysis of a single-axis rate gyro subjected to feedback control mounted on a space vehicle that is spinning with uncertain angular velocity ω_Z about its spin of the gyro is presented. For the autonomous case in which ω_Z is steady, we examine the dynamics of the resulting system on the center manifold near the double-zero degenerate point by using center manifold and normal form methods. There exist a few kinds of bifurcations in the autonomous case such as pitchfork and Hopf bifurcations for local bifurcation analyses, and a saddle-connection bifurcation for global analyses. As singular velocity ω_Z of the space vehicle is harmonic, the Melnikov technique was used to give criteria for the existence of chaos in the gyro motion. The numerical simulations are performed to verify the analytical results in the form of phase portraits, bifurcation diagrams and Lyapunov exponents. In addition, chaotic motions of this system can be changed into regular motions by a small parametric perturbation with Lyapunov exponent calculations.

1. INTRODUCTION

During the past few decades, chaotic dynamics of physical systems, which possess non-linearity and external excitation, have been extensively investigated. In gyroscopic systems, the dynamics of gyros also exhibit complex non-linear and chaotic behavior. Single-axis rate gyros are often used for the measurement of angular velocity in spinning space vehicles. The non-linear dynamics of a single-axis rate gyro mounted on a space vehicle with a variety of motion was widely analyzed by Singh [1] and Ge and Chen [2, 3]. For example, the motion of a single-axis rate gyro has been examined for small rotation θ of the gimbal when the angular velocity of vehicle is spinning about its spin axis [1]. The stability of a rate gyro mounted on a vehicle, which has a time-varying angular velocity about its spin of the gyro, was studied by Ge and Chen [2] using the Lyapunov direct method. The complex non-linear and chaotic motions of a rate gyro under harmonic excitation about the vehicle input axis were observed in reference [3]. All of them are two-dimensional systems. In this paper we will further study stability, double degeneracy and chaos in a rate gyro with feedback control that is a three-dimensional feedback system.

Holmes [4] used center manifold and normal form methods to study doubly degenerate local bifurcations of a single-degree-of-freedom system with non-linear stiffness, subjected to linear feedback control. Yagasaki [5] studied chaotic dynamics of a pendulum subjected to linear feedback control with periodic desired motion by applying Melnikov's method with the assistance of numerical computation. Li and Paidoussis [6] studied the chaotic dynamics of planar motions of cantilevered pipes conveying fluid via center manifold theory and the method of normal forms on the doubly degenerate point. The Melknikov analysis [7, 8] was used to give specific criteria for chaotic behavior in the non-autonomous

0022–460X/98/050753 + 17 $25.00/0/sv971281

system. In practice, chaotic motions are often undesirable. Lima and Pettini [9] used resonant parametric perturbations to change a chaotic regime into a regular one.

The stability and chaotic dynamics of a rate gyro system is shaded. A single-axis rate gyro subjected to feedback control are mounted on a space vehicle with specific motions and whether the spin axis of the rotor is parallel or opposite to the angular velocity of the vehicle in the system is considered. For the autonomous case, local bifurcation analyses reveal region of stability and bifurcation sequences with the associated phase portraits in the parametric space in the neighborhood of the double degeneracy. For the non-autonomous case, the dynamics are more complicated because the motions can be chaotic. A version of the Melnikov method is used to obtain criteria for the existence of chaotic motion for the reduced system. Finally, numerical results are presented to verify the analytical results. Chaotic motions are observed by the bifurcation diagrams and Lyapunov exponents and can be changed into regular motions by a small parameter perturbation with Lyapunov exponent calculations.

2. EQUATIONS OF MOTION

The model of a single-rate gyro mounted on a space vehicle is considered, as shown in Figure 1. The gimbal can turn about the outpux X-axis with rotational angle θ. Motion about this axis is resisted by damping torque defined by $C_d\dot{\theta}$. Using Lagrange's equation,

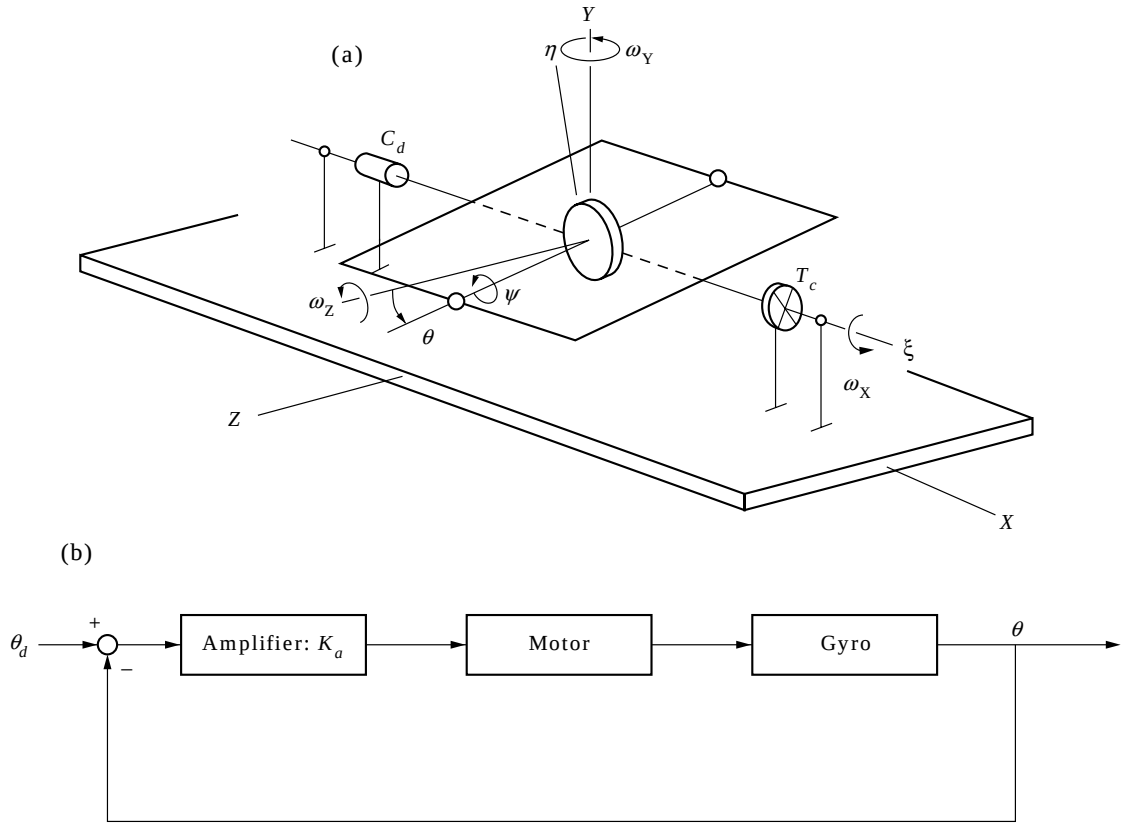

Figure 1. A rate gyro with feedback control.

the differential equation for the output deflection angle θ of a rate gyro with feedback control was derived [10]:

$$(A + A_g)\ddot{\theta} + C_d\,\dot{\theta} + Cn_R\,(\omega_Y \cos\theta + \omega_Z \sin\theta) + (A + B_g - C_g)\,(\omega_Y \cos\theta + \omega_Z \sin\theta)\,(\omega_Y \sin\theta - \omega_Z \cos\theta) + (A + A_g)\dot{\omega}_X = T_c, \tag{1}$$

where

$$Cn_R = C(\dot{\psi} - \omega_Y \sin\theta + \omega_Z \cos\theta) = \text{const.},$$

and ω_X, ω_Y and ω_Z denote the angular velocity components of the platform along output axis X, input axis Y, and normal axis Z, respectively. A, A, C and A_g, B_g and C_g denote the moments of inertia of rotor and gimbal, respectively, about the gimbal axes ξ, η and ζ. T_c is the control-motor torque along the output axis of the system to balance the corresponding gyroscopic torque. The torque and electric current of control-motor can be modelled by the following relationship:

$$T_c = K_T\,I, \qquad L\dot{I} + RI = K_a\,(\theta_d - \theta) - K_0\,\dot{\theta} \tag{2, 3}$$

where electromotive force proportional to the difference between the prescribed motion $\dot{\theta}_d\,(t)$ and the rotational angle θ, that is $u = K_a\,(\theta_d - \theta)$, is applied to the control-motor. I, R, L and K_0 are the current, resistance, inductance, and back-electromotive constant of the control-motor; K_T denotes the torque constant of the control-motor.

Equations (1)–(3) thus represent a feedback control system in which position feedback is applied to the gyro motion. The prescribed motion of the gyro is desired to be fixed at the origin, i.e., $\theta_d = 0$, in which the relationship of the output angle θ proportional to the input angular velocity ω_Y is held.

We are interested in the non-linear behavior of dynamical motion when the vehicle undergoes steady rotation about the X-axis, and the angular velocity about the input axis OY is zero, i.e., $\dot{\omega}_X = 0$ and $\omega_Y = 0$. The uncertain angular velocity about the spin axis of the gyro undergoes harmonic rotation with respect to the Z-axis, i.e., $\omega_Z = \kappa\omega_{Z0} + v \sin\omega t$. Here, two configurations of a rate gyro will be considered. In Case (a), the spin vector of the vehicle coincides with the spin vector of the gyro for $\theta = 0$, when $\kappa = 1$. In Case (b), the spin vector of the vehicle is opposite to the gyro spin for $\theta = 0$, when $\kappa = 1$. We assume that the angular velocity of the vehicle is slightly vibrating near a constant angular velocity.

The feedback control system can now be written in the form

$$\begin{aligned}
\dot{x}_1 &= x_2,\\
\dot{x}_2 &= -D_1\,x_2 + D_2\,x_3 - D_3\,\kappa\omega_{Z0} \sin x_1 + D_4\,\omega_{Z0}^2 \sin 2x_1\,/2 + v \sin\omega t(-D_3\,\kappa \sin x_1 + D_4\,\omega_{Z0} \sin 2x_1) + (v \sin\omega t)^2 D_4\,\omega_{Z0} \sin 2x_1\,/2,\\
\dot{x}_3 &= -D_5\,x_3 - D_6\,x_1 - D_7\,x_2,
\end{aligned} \tag{4}$$

where

$$x_1 = \theta, \qquad x_2 = \dot{\theta}, \qquad x_3 = I,$$

$$D_1 = C_d\,/(A + A_g), \qquad D_2 = K_T\,/(A + A_g), \qquad D_3 = Cn_R\,/(A + A_g),$$

$$D_4 = (A + B_g - C_g)/(A + A_g), \qquad D_5 = R/L, \qquad D_6 = K_a\,/L, \qquad D_7 = K_0\,/L,$$

and D_i, $i = 1, 2, \ldots, 7$, are known positive constants; let $x_1 = x$, $x_2 = y$ for plotting.

3. LOCAL BIFURCATION ANALYSIS

In this section, we will examine the qualitative behavior of this system in the neighborhood of a fixed point. Therefore we can express the original system in the Taylor series and keep the lowest-order non-linear terms to determine local phase portraits and stability types. The approximate system is given by

$$\begin{aligned}\dot{x}_1 &= x_2,\\ \dot{x}_2 &= -D_1 x_2 + D_2 x_3 + p_1 x_1 + p_2 x_1^3 + p_3 x_1 \sin \omega t,\\ \dot{x}_3 &= -D_5 x_3 - D_6 x_1 - D_7 x_2,\end{aligned} \tag{5}$$

where

$$p_1 = -D_3 \kappa\omega_{Z0} + D_4 \omega_{Z0}^2, \quad p_2 = (D_3 \kappa\omega_{Z0} - 4D_4 \omega_{Z0}^2)/6, \quad p_3 = v(-D_3 \kappa + 2D_4 \omega_{Z0}), \quad v \ll 1.$$

Here, consider a co-dimensional two bifurcation problem of the feedback system having double zero eigenvalues. The main purpose is to find the loci in the parametric plane and to observe the qualitative behaviors when the parameters are varied. Before proceeding to non-linear analysis, it is necessary to study the linear behavior of the system in order to determine critical parameter values from degenerate conditions. Linearizing at the fixed point and neglecting the perturbation ($v = 0$), we obtain the Jacobian matrix of the form

$$A = \begin{bmatrix} 0 & 1 & 0 \\ p_1 & -D_1 & D_2 \\ -D_6 & -D_7 & -D_5 \end{bmatrix}. \tag{6}$$

Hence, according to the Routh–Hurwitz criterion [10], the necessary and sufficient conditions are as follows

$$\omega_{Z1} < \omega_{Z0} < \omega_{Z2}, \tag{7}$$

where

$$\omega_{Z1} = \frac{D_3 - \sqrt{D_3^2 + 4D_4 p_{min}}}{2D_4}, \qquad \omega_{Z2} = \frac{D_3 + \sqrt{D_3^2 + 4D_4 p_{min}}}{2D_4},$$

and

$$p_{min} = \text{Min}\,[cond1, cond2]$$

$$cond1 = (D_1^2 D_5 + D_1 D_2 D_7 + D_1 D_5^2 - D_2 D_6 + D_2 D_5 D_7)/D_1$$

$$cond2 = D_2 D_6 / D_5$$

and all the roots of the characteristic polynomial of the Jacobian matrix (6) have negative real parts. This implies that the motion of the linearized autonomous system is asymptotically stable at the fixed point. Alternatively, the system possesses critical behavior when Jacobian matrix **A** contains the eigenvalues with zero real parts in the following bifurcation surfaces.

$p_1 = D_1 D_5 D_6 / (D_6 - D_5 D_7)$: one eigenvalue is zero at the origin;

$p_1 = (D_1^2 D_5 + D_1 D_2 D_7 + D_1 D_5^2 - D_2 D_6 + D_2 D_5 D_7)/D_1, \qquad D_2 (D_6 - D_5 D_7) > D_1 D_5^2$:

a pair of eigenvalues is pure imaginary at the origin.

These two surfaces meet on the surface (i.e., $\omega_{Z0} = \omega_{Z1}$ or ω_{Z2}, on stability boundary)

$$D_{2C} = D_1 D_5^2/(D_6 - D_5 D_7), \qquad p_{1C} = D_1 D_5 D_6/(D_6 - D_5 D_7), \tag{8}$$

where there is a doule-zero eigenvalue with the third eigenvalue being $-(D_1 + D_5)$. We consider a co-dimension two bifurcation problem. To transform the linear part of the system into the Jordan canonical form, we use the similarity transformation matrix of generalized eigenvectors of equation (6) as follows

$$T = \begin{bmatrix} 1 & a_{12} & a_{13} \\ 0 & 1 & a_{23} \\ a_{31} & 0 & 1 \end{bmatrix}, \tag{9}$$

where a_{12}, a_{13}, a_{23} and a_{31} are shown in Appendix A and its determinant is

$$\Delta = \det(T) = 1 - a_{13} a_{31} + a_{12} a_{23} a_{31}.$$

We introduce the parameters D_2 and p_1 in the forms

$$D_2 = D_{2C} + \varepsilon_1 = D_1 D_5^2/(D_6 - D_5 D_7) + \varepsilon_1 \tag{10}$$

$$p_1 = p_{1C} + \varepsilon_2 = D_1 D_5 D_6/(D_6 - D_5 D_7) + \varepsilon_2 \tag{11}$$

so that the unfolding of the critical system ($\varepsilon_1 = \varepsilon_2 = 0$) will be included in our parameterized normal form. Letting the co-ordinate transformation $y = Tx$, the system equation becomes the standard form

$$\dot{y} = \Lambda y + \Lambda_\varepsilon y + F_y + B_y(t) \tag{12}$$

where both the non-linear function F_y and the time-periodic perturbation $B_y(t)$ are evaluated at critical values; Λ, Λ_ε, F_y and $B_y(t)$ are shown in Appendix A.

In this case our goal is to study the system dynamics near this non-hyperbolic fixed point with a double-zero eigenvalue. By center manifold theory [11] the study of the dynamics can be reduced to the associated lower-dimensional center manifold to determine the key qualitative dynamics behavior. When the Jacobian matrix **A** about a fixed point contains a zero-double eigenvalue, the dimension of the center space is only two. Thus, if such a center manifold can be made, the subsequent analysis could be much easier.

The center manifold will compute from the standard form of equation (12) at the critical value ($\varepsilon_1 = \varepsilon_2 = 0$) for $v = 0$ ($p_3 = 0$). Thus, its computations will be confined to the autonomous form. For the angular velocity which is slightly vibrating, i.e., $v \ll 1$, excitation terms can be computed by the similarity transformation T as mentioned above. In section 4, the effect of parametric excitation will be considered by the Melnikov technique which can be used to detect the presence of homoclinic or heteroclinic orbits. Now we will begin by considering the center manifold for this system. Equation (5) contains cubic symmetry which implies that the center manifold will be given by an odd function $y_3 = h(y_1, y_2)$, i.e., $y_3 = O(|y_i^3|)$. Thus the corresponding reduced system is

$$\begin{bmatrix} \dot{y}_1 \\ \dot{y}_2 \end{bmatrix} = \begin{bmatrix} 0 & 1 \\ 0 & 0 \end{bmatrix} \begin{bmatrix} y_1 \\ y_2 \end{bmatrix} + \begin{bmatrix} e_{11} & e_{12} \\ e_{21} & e_2 \end{bmatrix} \begin{bmatrix} y_1 \\ y_2 \end{bmatrix} + \begin{bmatrix} f_{yc1} \\ f_{yc2} \end{bmatrix} + \begin{bmatrix} b_{yc1} \\ b_{yc2} \end{bmatrix} + h.o.t., \tag{13}$$

where $h.o.t.$ are of orders $O(|y_i^5|)$, $O(|\varepsilon_i y_i^3|)$, $(|\varepsilon_i^2 y_i|)$, and $O(|v\varepsilon_i y_i|)$ and the relevant symbols are defined in Appendix A.

To put equation (13) into a more convenient form we employ a linear change of co-ordinates

$$\begin{bmatrix} y_1 \\ y_2 \end{bmatrix} = \begin{bmatrix} 1 + e_{12} & 0 \\ -e_{11} & 1 \end{bmatrix} \begin{bmatrix} u_1 \\ u_2 \end{bmatrix}, \tag{14}$$

which yield the system

$$\begin{aligned} \dot{u}_1 &= u_2 + f_{u1} + b_{u1} + h.o.t., \\ \dot{u}_2 &= \mu_1 u_1 + \mu_2 u_2 + f_{u2} + b_{u2} + h.o.t., \end{aligned} \tag{15}$$

where μ_1, μ_2, f_{u1}, f_{u2}, b_{u1} and b_{u2} are defined in Appendix A.

At this stage, the method of normal forms is employed to simplify the reduced system in which the qualitative dynamics are still reserved in the neighborhood of the origin. The basic idea of normal forms is to use a near-identity co-ordinate transformation in which all non-essential non-linear terms are eliminated. Thus, the truncated normal form is given by

$$\begin{aligned} \dot{z}_1 &= z_2 + (k_1 z_1 + k_{12} z_2) \sin \omega t, \\ \dot{z}_2 &= \mu_1 z_1 + \mu_2 z_2 + a z_1^3 + b z_1^2 z_2 + (k_{21} z_1 + k_{22} z_2) \sin \omega t, \end{aligned} \tag{16}$$

where the relevant symbols are defined in Appendix A.

We directly deduce the dynamical behavior of the full system (12) on the center manifold near the critical degenerate system. At this stage, the rescaling technique can be used to reduce the number of cases. Letting $z_1 \to r_1 z_1$, $z_2 \to r_2 z_2$ and $t \to r_3 t$, we obtain

$$\begin{aligned} \dot{z}_1 &= z_2 + (k'_{11} z_1 + k'_{12} z_2) \sin \omega' t, \\ \dot{z}_2 &= \mu'_1 z_1 + \mu'_2 z_2 + c z_1^3 - z_1^2 z_2 + (k'_{21} z_1 + k'_{22} z_2) \sin \omega' t, \end{aligned} \tag{17}$$

where

$$\mu'_1 = \mu_1 r_3^2, \quad \mu'_2 = \mu_2 r_3, \quad k'_{11} = k_{11} r_3, \quad k'_{12} = k_{12}, \quad k'_{21} = k_{21} r_3^2,$$

$$k'_{22} = k_{22} r_3, \quad \omega' = r_3 \omega, \quad r_1 = (a/c)^{1/2}/b, \quad r_2 = -(a/c)^{3/2}/b^2, \quad r_3 = -(bc/a),$$

and $c = +1$ for $a > 0$, $c = -1$ for $a < 0$. There are two distinct cases ($c = \pm 1$) to be considered.

The autonomous system

$$\begin{aligned} \dot{z}_1 &= z_2, \\ \dot{z}_2 &= \mu'_1 z_1 + \mu'_2 z_2 + c z_1^3 - z_1^2 z_2, \end{aligned} \tag{18}$$

is considered, which is obtained by letting $p_3 = 0$. By local bifurcation analysis, the system (18) has been studied quite extensively (Appendix B). We can consequently employ the unfolding results of references [4, 8] directly to give the dynamical behavior of the full system (5) on the center manifold near the critical degenerate.

4. THE MELNIKOV ANALYSIS

From the autonomous system as mentioned above, a pair of symmetric heteroclinic orbits exist on the curve $\mu'_2 = -\mu'_1/5 + O(\mu'^2_1)$ for $c = +1$, and a pair of symmetric homoclinic orbits exist on the curve $\mu'_2 = 4\mu'_1/5 + O(\mu'^2_1)$ for $c = -1$. If the system has perturbations, i.e., $p_3 \neq 0$, this system becomes non-autonomous, and these heteroclinic or

homoclinic orbits may be broken. At this stage, we suspect the existence of transverse heteroclinic or homoclinic orbits in this system.

For $c = +1$, using the rescaling $z_1 = \varepsilon u$, $z_2 = \varepsilon^2 v_1$, $\mu_1' = -\varepsilon^2$, $\mu_2' = \varepsilon^2 v_3 = -\mu_1' v_3$, $p_3 = \varepsilon^3 p$, $t \to \varepsilon t$ and neglecting higher order terms of ε, the rescaled form of system (17) is given by

$$\dot{u} = v_1,$$

$$\dot{v}_1 = -u + u^3 + \epsilon(v_3 v_1 - u^2 v_1 + ku \sin \hat{\omega} t) \tag{19}$$

where $\hat{\omega} = \epsilon\omega'$.

For $\varepsilon = 0$, system (19), which has a center at $(0, 0)$ and hyperbolic saddles at $(\pm 1, 0)$, is a Hamiltonian system with Hamiltonian function

$$H(u, v_1) = v_1^2/2 + u^2/2 - u^4/4. \tag{20}$$

The Hamiltonian system has heteroclinic orbits that connect different saddle points. Hence the hyperbolic periodic orbits of the Hamiltonian system are given by

$$q_h^{\pm}(t) = (q_{1h}^{\pm}, q_{2h}^{\pm}) = (\pm \tanh t, \pm \operatorname{sec} h^2 t/\sqrt{2}). \tag{21}$$

We will compute the Melnikov function for q_h^+ (the computation for q_h^- is identical). The Melnikov function is given by [7]

$$M^+(t_0) = \int_{-\infty}^{\infty} f(q_h^+(t)) \hat{} g(q_h^+(t), t + t_0)\, \mathrm{d}t$$

$$= \int_{-\infty}^{\infty} q_{2h}^+(t)\,[v_3 q_{2h}^+(t) - q_{1h}^+(t)^2 q_{2h}^+(t) + k q_{1h}^+(t) \sin \hat{\omega}(t + t_0)]\, \mathrm{d}t$$

$$= \frac{2}{3} v_3 - \frac{2}{15} - \frac{k\pi\hat{\omega}^2}{2\sqrt{2}} \operatorname{csc} h\left(\frac{\hat{\omega}^2\pi}{2}\right) \cos \hat{\omega} t_0. \tag{22}$$

For $c = -1$, using the rescaling $z_1 = \varepsilon u$, $z_2 = \varepsilon^2 v_1$, $\mu_1' = \varepsilon^2$, $\mu_2' = \varepsilon^2 v_3 = \mu_1' v_3$, $p_3 = \varepsilon^3 p$, $t \to \varepsilon t$, and neglecting higher order terms of ε, the rescaled form of system (17) is given by

$$\dot{u} = v_1,$$

$$\dot{v}_1 = u - u^3 + \varepsilon(v_3 v_1 - u^2 v_1 + ku \sin \hat{\omega} t). \tag{23}$$

For $\varepsilon = 0$, system (23), which has centers at $(\pm 1, 0)$ and a hyperbolic saddle at $(0, 0)$, is a Hamiltonian system with Hamiltonian function

$$H(u, v_1) = v_1^2/2 - u^2/2 + u^4/4. \tag{24}$$

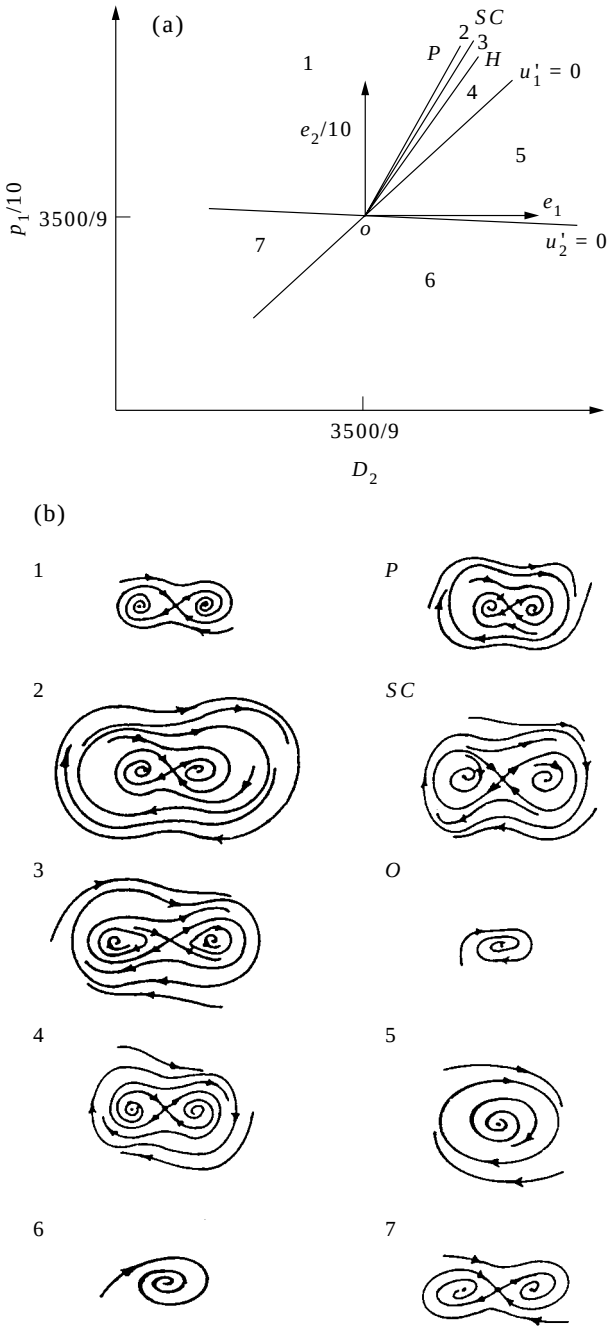

Figure 2. Bifurcation diagram near (D_{2C}, p_{1C}): (a) Bifurcation set in (D_2, p_1) space; (b) the associated phase portraits; H: Hopf bifurcation, SC: saddle connection bifurcation, P: saddle-node bifurcation of cycles, $\mu_1' = 0$: pitchfork bifurcation.

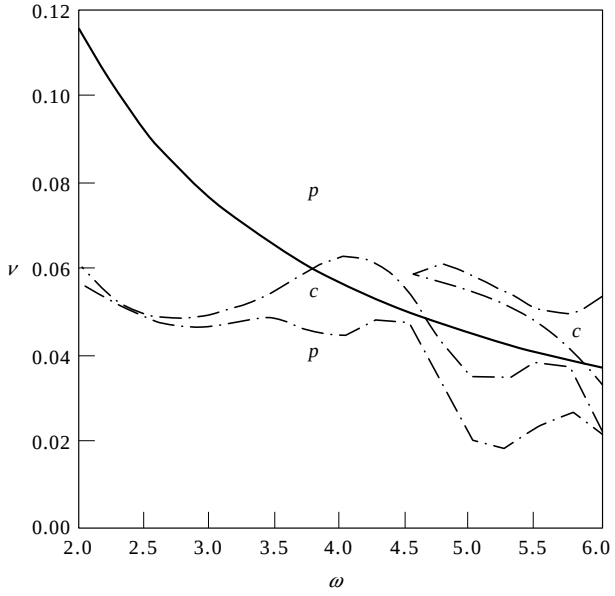

Figure 3. Parametric diagram and the Melnikov criterion in $(\omega - v)$ plane; p: the region of periodic motion, c: the region of chaotic motion.

The Hamiltonian system has homoclinic orbits that connect a saddle point. Hence the hyperbolic periodic orbits of the Hamiltonian system are given by

$$q_h^{\pm}(t) = (q_{1h}^{\pm}, q_{2h}^{\pm}) = (\pm\sqrt{2}\,\sec ht, \mp\sqrt{2}\,\sec ht\,\tanh t). \tag{25}$$

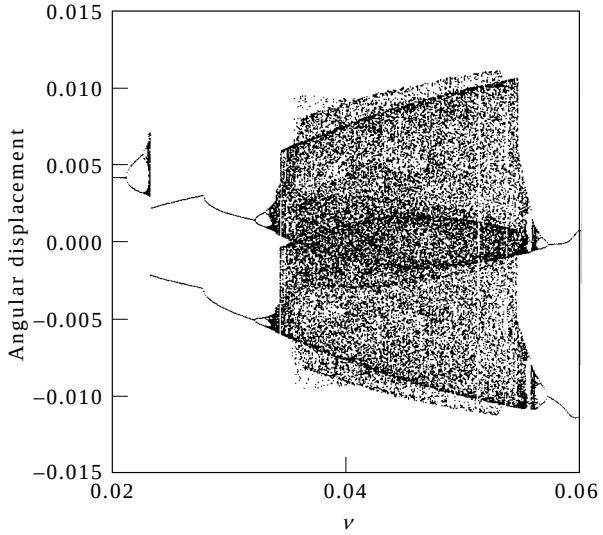

Figure 4. Bifurcation diagram for the pulsatile angular velocity; $\omega = 6{\cdot}0$.

We will compute the Melnikov function for q_h^+. The Melnikov function is given by

$$M^+(t_0) = \int_{-\infty}^{\infty} f(q_h^+(t)) \hat{} g(q_h^+(t), t + t_0)\, \mathrm{d}t$$

$$= \int_{-\infty}^{\infty} q_{2h}^+(t)\,[v_3\, q_{2h}^+(t) - q_{1h}^+(t)^2 q_{2h}^+(t) + k q_{1h}^+(t) \sin \hat{\omega}(t + t_0)]\, \mathrm{d}t$$

$$= \frac{4}{3} v_3 - \frac{16}{15} - \pi\hat{\omega}^2 \operatorname{csc} h\left(\frac{\hat{\omega}\pi}{2}\right) \cos \hat{\omega} t_0. \tag{26}$$

Suppose that $M^+(t_0)$ has a simple zero, i.e., there exists a point $t_0 = \bar{t}_0$ such that

$$M^+(\bar{t}_0), \qquad \frac{\partial M^+}{\partial t_0}(\bar{t}_0) \neq 0. \tag{27}$$

For $c = +1$, the stable and unstable perturbed manifolds that are close to heteroclinic manifolds of the unperturbed system intersect transversely, and there exist transverse heteroclinic orbits at certain parameter values and some t_0. For $c = -1$, the stable and unstable perturbed manifolds intersect transversely and there exist transverse homoclinic orbits. It follows from the Melnikov theory that if the forcing amplitude

$$k > R_1(\hat{\omega}) = \left| \left(\frac{2}{3} v_3 - \frac{2}{15}\right) \Big/ \left[\frac{\pi\hat{\omega}^2}{2\sqrt{2}} \operatorname{csc}\left(\frac{\pi\hat{\omega}^2}{2}\right)\right] \right| \qquad \text{for } c = +1, \tag{28}$$

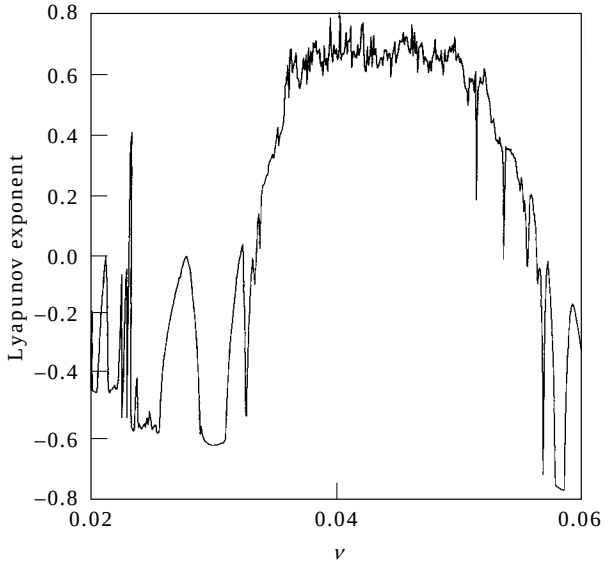

Figure 5. Lyapunov diagram for the pulsatile angular velocity; $\omega = 6{\cdot}0$.

$$k > R_2(\hat{\omega}) = \left| \left(\frac{4}{3} v_3 - \frac{16}{15} \right) \Big/ \left[\pi \hat{\omega}^2 \csc\left(\frac{\pi \hat{\omega}}{2} \right) \right] \right| \quad \text{for } c = -1, \tag{29}$$

the manifolds of the equations (19) and (23) intersect and may yield horseshoe maps near the saddle points. (Equation (29) is numerically computed at the specific values of gyro parameters and the result is shown in Figure 3).

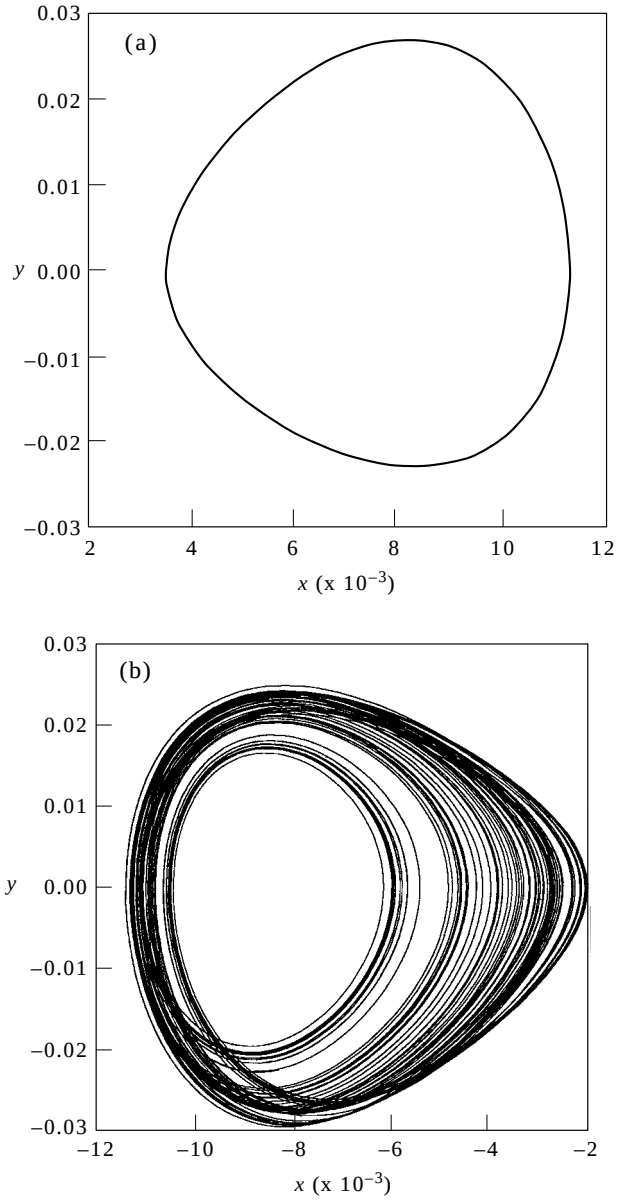

Fig. 6a–b. (*Caption on p.* 000.)

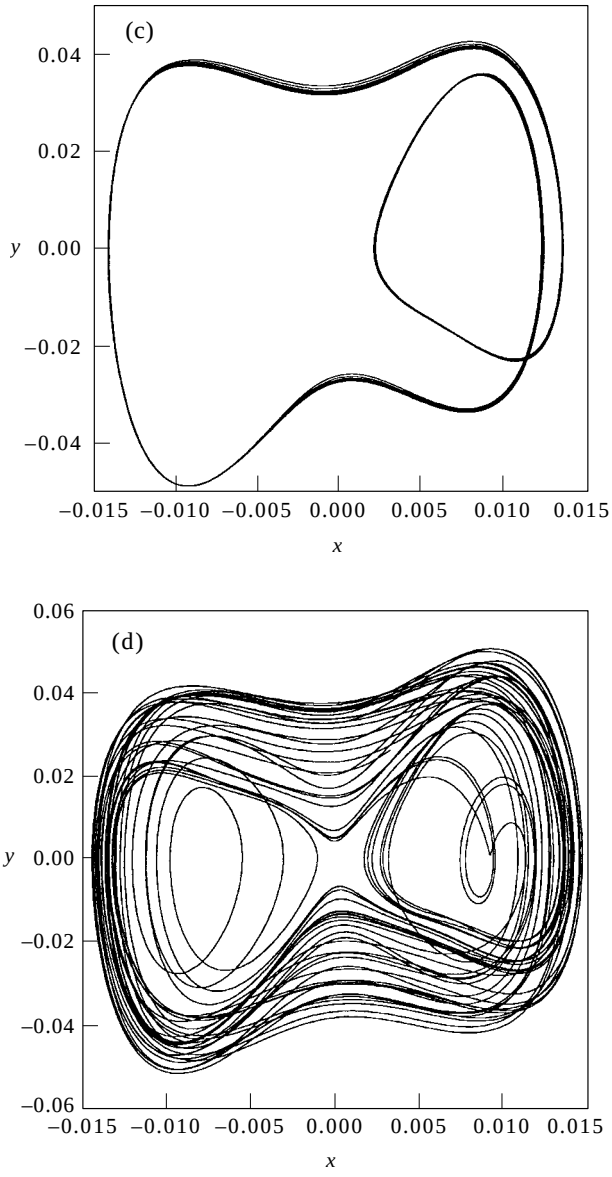

Fig. 6(c–d).

Figure 6. Phase portraits, corresponding to the bifurcation diagram of Figure 5, showing (a) a periodic motion for $v = 0{\cdot}02$, (b)–(d) chaotic motions for $v = 0{\cdot}023$, $0{\cdot}035$ and $0{\cdot}04$, respectively.

5. NUMERICAL DEMONSTRATIONS

In this section, examples are carried out to examine the vibration behavior by numerical simulation technique for the double-zero degenerate case. The parameters of the cases are shown in Appendix C.

We first examine the dynamics of the autonomous system (5) with $v = 0$ on the center manifold near the double-zero degenerate point $(D_{2C}, p_{1C}) = (388{\cdot}89, 3888{\cdot}9)$. In Figure 2 we illustrate a bifurcation set in (D_2, p_1) space for equation (18), $c = -1$, with the associated phase portraits which are topologically equivalent to the flow on the center

manifold. The local bifurcation analyses for the full system (4) can be studied through system (5), which keeps the lowest-order non-linear terms, by the center manifold and normal form methods.

Later the dynamics of the non-autonomous system (5) are studied. For the parameters near degenerate point $(D_2, p_1) = (D_{2C} + \epsilon_1, p_{1C} + \epsilon_2) = (388{\cdot}89, 4036{\cdot}6)$, i.e., $\omega_{Z0} = 2002{\cdot}016258$, from the results of the Melnikov analysis of section 4, the function $v(\omega)$ is numerically computed as the solid curve in Figure 3. Figure 3 also shows the regions of chaos enclosed between two dash–dot curves by numerical integration and the solid curve gives a lower-bound on chaotic behavior by analytical means, but it is not a good approximation for the case. It should be pointed out that the discussion of possible chaotic motions in the full system is certainly not in agreement with the analysis of the two-dimensional subsystems. Furthermore, the relationship of chaotic dynamics and heteroclinic bifurcation ($c = +1$) or homoclinic bifurcation ($c = -1$) in higher dimensional space is still imperfectly understood. Hence, we present the numerical results to explore this difficult problem.

The bifurcation diagram in Figure 4 shows the long-term values of the rotational angle at the fixed driving frequency $\omega = 6{\cdot}0$, by numerical integration from equation (4). The largest Lyapunov exponents for each value of the driving amplitude v are also computed corresponding to the bifurcation diagram to definitely show the existence of chaos as shown in Figure 5. Obviously, the random-like distributions of points in the bifurcation diagram which have positive exponents are indeed chaotic.

To further confirm the results in Figure 4, we examine phase portraits for some special values of v. The phase portrait in Figure 6(a) is a period-T ($T = 2\pi/\omega$) attractor for $v = 0{\cdot}02$. Figure 5(b)–(d), which have positive Lyapunov exponents, show chaotic motions in the phase portraits for $v = 0{\cdot}023$, $0{\cdot}035$ and $0{\cdot}04$, respectively. In Figure 6(b) and (c) the chaotic motion occurs through a series of period-doubling bifurcations. There exists a pair of chaotic attractors which have inverted onto the (x, y)-plane, i.e., $(x, y) = (-x, -y)$ so that one of them can be reached depending on initial conditions.

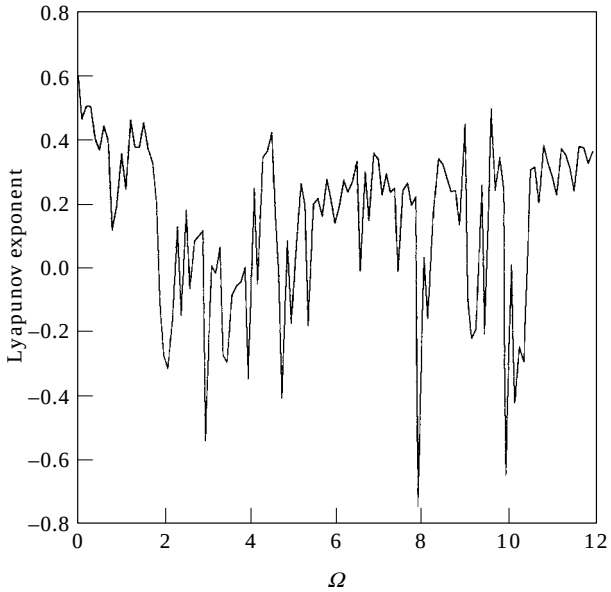

Figure 7. The largest Lyapunov exponent as a function of Ω for $D_2 = D_{2C}(1 + \eta \sin \Omega t)$; $\omega = 6{\cdot}0$, $v = 0{\cdot}04$ and $\eta = 0{\cdot}1$.

Increasing the parameter v, conjunction of the two chaotic attractors, one of them as shown in Figure 6(c) creates a larger chaotic attractor in Figure 6(d).

Physically, chaos may be desirable or undesirable, depending on the application. In mechanical systems, chaos may lead to irregular motions, so it has to be reduced or suppressed. In this case, we can use a small parametric perturbation with the assistance of the Lyapunov exponent calculations to bring the system from a chaotic regime to a regular one. Changing the parameter D_2 as $D_2(1 + \eta \sin \Omega t)$, $\eta = 0{\cdot}1$, there is a spectrum of the largest Lyapunov exponents λ_{max} as the function of the frequency Ω in Figure 7. As $\lambda_{max} < 0$ for the suitable frequency Ω, the system is periodic. On the other hand, increasing

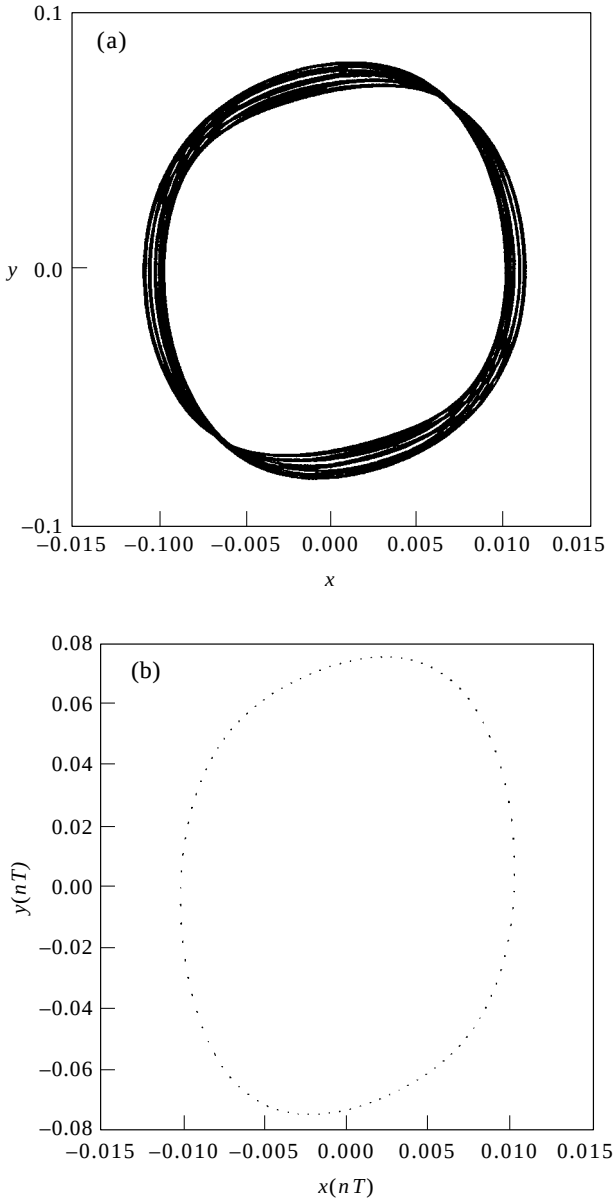

Figure 8. A quasi-periodic attractor, as $D_2 = D_{2C}(1 + \eta)$, $\omega = 6{\cdot}0$, $v = 0{\cdot}04$ and $\eta = 0{\cdot}1$, plotted in (a) phase plane, (b) Poincaré maps.

the gain D_2 of this system as $D_2(1+\eta)$, $\eta = 0{\cdot}1$, the chaotic system becomes only quasi-periodic as shown in Figure 8.

6. CONCLUSIONS

An analysis is presented of a single-axis rate gyro subjected to feedback control mounted on a space vehicle that is spinning with uncertain angular velocity ω_Z about its spin of the gyro. The dynamics of the system are investigated near doubly degenerate points by using center manifold and normal form methods. These methods can reduce the dynamics to a simpler form which still retains the essentials of dynamical behavior of the original system.

In section 3, the autonomous system (steady angular velocity ω_Z) reveals the existence of saddle connection, pitchfork, and Hopf bifurcations near the double degeneracy by local bifurcation analyses. A bifurcation set and the associated sequence of phase portraits on the center manifold are presented. For the non-autonomous system, Melnikov analysis is applied to the reduced system to show the existence of chaotic motion in section 4.

Finally, to confirm the analytical results of sections 4 and 5, simulations are presented in section 6 with the full system for the autonomous and non-autonomous systems. The occurrence of the chaotic motion of the full system is also detected by calculating bifurcation diagrams and Lyapunov exponents. In addition, we consider a small parametric perturbation to change a chaotic motion into a regular motion in this system by computing Lyapunov exponents.

REFERENCES

1. S. N. Singh 1983 *IEEE Transactions on Aerospace and Electronic Systems* **AES-19**, 182–189. Stability of gyro with harmonic nonlinearity in spinning vehicle.
2. Z. M. Ge and C. J. Chen 1992 *AIAA Journal of Guidance, Control, and Dynamics* **15**, 1034–1036. Stability of a rate gyro.
3. Z. M. Ge and H. H. Chen 1996 *Journal of Sound and Vibration* **194**, 107–117. Bifurcations and chaos in a rate gyro with harmonic excitation.
4. P. Holmes 1985 *Trans. ASME J. Dyn. Sys. Meas. Control* **107**, 159–165. Dynamics of a nonlinear oscillator with feedback control I: local analysis.
5. K. Yagasaki 1994 *Nonlinear Dynamics* **6**, 125–142. Chaos in a pendulum with feedback control.
6. G. X. Li and M. P. Paidoussis 1949 *International Non-Linear Mechanics* **29**, 83–107. Stability, double degeneracy and chaos in cantilevered pipes conveying fluid.
7. S. Wiggins 1988 *Global Bifurcations and Chaos*. New York: Springer-Verlag.
8. J. Guckenheimer and P. Holmes 1986 *Nonlinear Oscillations, Dynamical Systems and Bifurcation of Vector Fields*. New York: Springer-Verlag.
9. R. Lima and M. Pettini 1990 *Physical Review A* **41**, 726–733. Suppression of chaos by resonant parametric perturbations.
10. L. Meirovitch 1970 *Method of Analytical Dynamics*. New York: McGraw-Hill.
11. J. Carr 1981 *Application of Center Manifold Theory*. New York: Springer-Verlag.

APPENDIX A

$$a_{12} = -(-D_6 + D_5 D_7)/(D_5 D_6),$$

$$a_{13} = D_1/D_6 - D_1(D_1 + D_5)D_7/(D_6(-D_6 + (D_1 + D_5)D_7)),$$

$$a_{23} = D_1(D_1 + D_5)/(-D_6 + (D_1 + D_5)D_7), \qquad a_{31} = -D_6/D_5.$$

$$\Lambda = \begin{bmatrix} 0 & 1 & 0 \\ 0 & 0 & 0 \\ 0 & 0 & -D_1 - D_5 \end{bmatrix}, \qquad \Lambda_\epsilon = \begin{bmatrix} e_{11} & e_{12} & e_{13} \\ e_{21} & e_{22} & e_{23} \\ e_{31} & e_{32} & e_{33} \end{bmatrix}, \qquad F_y = T^{-1}F(Ty) = \begin{bmatrix} f_{y1} \\ f_{y2} \\ f_{y3} \end{bmatrix},$$

$$B_y(t) = T^{-1}BTy = \begin{bmatrix} b_{y1} \\ b_{y2} \\ b_{y3} \end{bmatrix},$$

$$e_{11} = -a_{12}(a_{31}e_1 + e_2)/\Delta, \qquad e_{12} = -a_{12}^2 e_2/\Delta, \qquad e_{13} = -a_{12}(e_1 + a_{13}e_2)/\Delta,$$

$$e_{21} = (1 - a_{13}a_{31})(a_{31}e_1 + e_2)/\Delta, \qquad e_{22} = a_{12}(1 - a_{13}a_{31})e_2/\Delta,$$

$$e_{23} = (1 - a_{13}e_{31})(e_1 + a_{13}e_2)/\Delta,$$

$$e_{31} = a_{12}a_{31}(a_{31}e_1 + e_2)/\Delta, \qquad e_{32} = a_{12}^2 a_{31}e_2/\Delta, \qquad e_{33} = a_{12}a_{31}(e_1 + a_{13}e_2)/\Delta,$$

$$f_{y0} = p_2(y_1 + a_{12}y_2 + a_{13}y_3)^3/\Delta, \qquad f_{y1} = -a_{12}f_{y0}, \qquad f_{y2} = (1 - a_{13}a_{31})f_{y0},$$

$$f_{y3} = a_{12}a_{31}f_{y0},$$

$$b_{y0} = p_3(y_1 + a_{12}y_2 + a_{13}y_3)\sin\omega t/\Delta, \qquad b_{y1} = -a_{12}b_{y0}, \qquad b_{y2} = (1 - a_{13}a_{31})b_{y0},$$

$$b_{y3} = a_{12}a_{31}b_{y0}.$$

$$f_{yc0} = p_2(y_1 + a_{12}y_2)^3/\Delta, \qquad f_{yc1} = -a_{12}f_{yc0}, \qquad f_{yc2} = (1 - a_{13}a_{31})f_{yc0},$$

$$b_{yc0} = p_3(y_1 + a_{12}y_2)\sin\omega t/\Delta, \qquad b_{yc1} = -a_{12}b_{yc0}, \qquad b_{yc2} = (1 - a_{13}a_{31})b_{yc0}.$$

$$\mu_1 = e_{21} = [(1 - a_{13}a_{31})a_{31}/\Delta]e_1 + [(1 - a_{13}a_{31})/\Delta]e_2,$$

$$\mu_2 = e_{11} + e_{22} = -(a_{12}a_{31}/\Delta)e_1 - (a_{12}a_{13}a_{31}/\Delta)/e_2,$$

$$f_{u0} = p_2(u_1 + a_{12}u_2)^3/\Delta, \qquad f_{u1} = -a_{12}f_{u0}, \qquad f_{u2} = (1 - a_{13}a_{31})f_{u0},$$

$$b_{u0} = p_3(u_1 + a_{12}u_2)\sin\omega t/\Delta, \qquad b_{u1} = -a_{12}b_{u0}, \qquad b_{u2} = (1 - a_{13}a_{31})b_{u0},$$

$$a = p_2(1 - a_{13}a_{31})/\Delta, \qquad b = -3p_2a_{12}a_{13}a_{31}/\Delta,$$

$$k_{11} = -p_3a_{12}/\Delta, \qquad k_{12} = -p_3a_{12}^2/\Delta,$$

$$k_{21} = p_3(1 - a_{13}a_{31})/\Delta, \qquad k_{22} = p_3a_{12}(1 - a_{13}a_{31})/\Delta.$$

APPENDIX B

Here, only an outline of the basic information needed for our special purpose is given by reference [7]. First, the system equilibrium points are determined as follows

$$c = +1\text{: } (0, 0), (\pm\sqrt{-\mu_1'}, 0), \qquad c = -1\text{: } (0, 0), (\pm\sqrt{\mu_1'}, 0),$$

By checking the linearized stability for these fixed points, the following bifurcation sets occur.

$$c = +1\text{: pitchfork on } \mu_1' = 0,$$

$$\text{supercritical Poincaré–Andronov–Hopf on } \mu_1' < 0, \mu_2' = 0.$$

$$c = -1\text{: pitchfork on } \mu_1' = 0,$$

$$\text{subcritical Poincaré–Andronov–Hopf on } \mu_1' = \mu_2', \mu_2' > 0.$$

By using Bendixson's criterion and index theory, equation (18) has no periodic orbits for

$$c = +1\text{: } \mu_1' > 0; \qquad \mu_1' < 0, \mu_2' < 0, \qquad \mu_2' > -\mu_1'/5, \mu_1' < 0.$$

$$c = -1\text{: } \mu_2' < 0.$$

The results above are shown in Figure 2 for $c = -1$.

In addition the pitchfork and Hopf bifurcations for local analyses, a saddle-connection or homoclinic bifurcation for global analyses is considered below to complete the bifurcation diagram.

For $c = +1$, using the rescaling $z_1 = \epsilon u$, $z_2 = \epsilon^2 v_1$, $\mu_1' = -\epsilon^2$, $\mu_2' = \epsilon^2 v_2$ and $t \to \epsilon t$, the rescaled form of system (18) is given by

$$\dot{u} = v_1,$$

$$\dot{v}_1 = -u + u^3 + \epsilon(v_2 v_1 - u^2 v_1). \tag{B1}$$

For $\epsilon = 0$, the system (B1) is a Hamiltonian system with Hamiltonian function

$$H(u, v_1) = v_1^2/2 + u^2/2 - u^4/4. \tag{B2}$$

By using the Melnikov theory, the autonomous system has a heteroclinic connection on

$$\mu_2' = -\mu_1'/5 + O(\mu_1'^2). \tag{B3}$$

For $c = -1$, using the rescaling $z_1 = \epsilon u$, $z_2 = \epsilon^2 v_1$, $\mu_1' = \epsilon^2$, $\mu_2' = \epsilon^2 v_2$ and $t \to \epsilon t$, the rescaled form of system (18) is given by

$$\dot{u} = v_1, \qquad \dot{v}_1 = u - u^3 + \epsilon(v_2 v_1 - u^2 v_1). \tag{B4}$$

For $\epsilon = 0$, the system (B4) is a Hamiltonian system with Hamiltonian function

$$H(u, v_1) = v_1^2/2 - u^2/2 + u^4/4. \tag{B5}$$

By using the Melnikov theory, the autonomous system has a homoclinic bifurcation on

$$\mu_2' = 4\mu_1'/5 + O(\mu_1'^2)$$

and a saddle-node bifurcation of cycles on $\mu_2' = d\mu_1' + \cdots$, $d \approx 0{\cdot}752$, on which the periodic orbits coalesce.

APPENDIX C

The values of gyro parameters:

$$\kappa = 1,$$

$$(A + A_g) = 54 \text{ dyne} \cdot \text{cm} \cdot \text{s}^2, \qquad Cn_R = 10{\cdot}8 \times 10^4 \text{ dyne} \cdot \text{cm} \cdot \text{s},$$

$$C_d = 7560 \text{ dyne} \cdot \text{cm} \cdot \text{rad}^{-1}\,\text{s},$$

$$D_1 = \frac{C_d}{(A + A_g)} = 140 \text{ rad}^{-1} \cdot \text{s}^{-1}, \quad D_3 = \frac{Cn_R}{(A + A_g)} = 2000 \text{ s}^{-1}, \quad D_4 = \frac{(A + B_g - C_g)}{(A + A_g)} = 1,$$

$$D_5 = R/L = 25 \text{ sec}^{-1}, \qquad D_6 = K_a/L = 250 \text{ A} \cdot \text{rad}^{-1} \cdot \text{s}^{-1}, \qquad D_7 = K_0/L = 1 \text{ A} \cdot \text{rad}^{-1}$$